Physical properties of ceramides: effect of fatty acid hydroxylation

Jyotsna Shah, Josephine M. Atienza, Anthony V. Rawlings,* and G. Graham Shipley[1]

Departments of Biophysics and Biochemistry, Center for Advanced Biomedical Research, Boston University School of Medicine, Boston, MA 02118, and Unilever Research U.S. Edgewater Laboratory,* Edgewater, NJ 07020

Abstract The structural and thermotropic properties of α-hydroxy fatty acid (HFA) and non-hydroxy fatty acid (NFA) ceramides (CER) have been studied using differential scanning calorimetry (DSC) and X-ray diffraction techniques. The DSC of anhydrous HFA-CER shows a single, sharp reversible transition at 95.6°C (ΔH = 15.3 kcal/mol). At intermediate hydrations HFA-CER exhibited more complex behavior but at maximum hydration only a single reversible transition is observed at 80.0°C (ΔH = 8.5 kcal/mol). X-ray diffraction of hydrated (74% water) HFA-CER at 20°C shows a lamellar structure with a bilayer periodicity d = 60.7 Å; a single wide angle reflection at 4.2 Å is characteristic of hexagonal chain packing. Above the main transition temperature at 91°C, a hexagonal (H_{II}) phase is observed. In contrast, DSC of anhydrous NFA-CER demonstrates two thermal transitions at 81.3°C (ΔH = 6.8 kcal/mol) and 85.9°C (ΔH = 3.5 kcal/mol). With increasing hydration, both transitions shift towards lower temperatures; at maximum hydration, on heating, the endothermic transitions occur at 72.7°C (ΔH = 9.8 kcal/mol) and 81.1°C (ΔH = 4.0 kcal/mol). On cooling, there is hysteresis of both transitions. X-ray diffraction of NFA-CER (80% water) at 20°C shows a well-ordered lamellar structure with a bilayer periodicity d = 58.6 Å and three wide-angle reflections at 4.6 Å, 4.2 Å, and 3.8 Å. At 77°C (between the two transitions), again a lamellar structure exists with reduced bilayer periodicity d = 53.1 Å and four wide-angle reflections at 4.6 Å, 4.2 Å, and 3.8 Å are observed. Above the second transition, only a single low angle reflection at 30.0 Å is observed; a diffuse reflection at 4.6 Å is indicative of a melted chain phase. Thus, HFA-CER exhibits a simple phase behavior involving the reversible conversion of a gel phase to a hexagonal phase ($L_\beta \rightarrow H_{II}$). However, NFA-CER shows a more complex polymorphic phase behavior involving two gel phases.—**Shah, J., J. M. Atienza, A. V. Rawlings, and G. G. Shipley.** Physical properties of ceramides: effect of fatty acid hydroxylation. *J. Lipid Res.* 1995. **36:** 1945–1955.

Supplementary key words sphingolipids • cell signaling • second messengers • stratum corneum • X-ray diffraction • scanning calorimetry • bilayers • phase transitions

The bilayer lipid matrix of cell membranes is composed of a heterogeneous mixture of different lipids, e.g., phospholipids, sphingolipids, and cholesterol. With the exception of sphingomyelin, sphingolipids are usually minor components of membranes. However, the sphingolipids and their breakdown products are now thought to be involved in various cellular processes, e.g., transport functions, immunological activity, cell growth, and differentiation (1–5). Consequently, there is a growing interest in the structure and properties of sphingolipids (6–8).

The essential molecular features of sphingolipids are *i)* a hydrophobic backbone called ceramide, which consists of a sphingosine base with an amide-linked fatty acid and *ii)* a polar head group. Ceramide itself is synthesized in the endoplasmic reticulum and transported to the Golgi apparatus where it is converted to cerebroside, ganglioside, or sphingomyelin (9). Although ceramide acts as a precursor for cerebroside, ganglioside, and sphingomyelin, very low levels of free ceramide are found in membranes.

Recently, it has been demonstrated that certain environmental signals that induce cell growth inhibition, cell differentiation, programmed cell death (apoptosis), and down-regulation of the c-myc protooncogene rapidly increase intracellular ceramide concentrations by increasing sphingomyelin turnover or by increasing de novo synthesis (10–17). A role for the generated ceramide in mediating some of the activities of these extracellular signals (e.g., tumor necrosis factor-α (TNF-α), γ-interferon or 1-α, 25-dihydroxyvitamin D_3) was demonstrated with the use of water-soluble, cell-permeable ceramide analogues (11, 13, 18, 19). These studies have established a potential signaling pathway involving sphingomyelin hydrolysis with the generation of a puta-

Abbreviations: HFA-CER, hydroxy fatty acid ceramide; NFA-CER, non-hydroxy-fatty acid ceramide; DSC, differential scanning calorimetry; TLC, thin layer chromatography.

[1]To whom correspondence should be addressed.

tive second messenger molecule, ceramide. Ceramides have been shown to induce phosphorylation of the EGF receptor possibly by activating a protein kinase (20, 21). A novel ceramide-activated protein phosphatase has been identified that may be involved in transducing the effects of ceramide (14, 22–24). Thus, the second messenger ceramide can dispatch the signal via activation of a protein kinase or a protein phosphatase.

In addition, it has been long known that the permeability barrier of skin, which prevents the water loss and penetration of the harmful chemicals from the environment, is localized in the horny layer (stratum corneum) of the epidermis (25, 26). Ceramides are present in large amounts in the stratum corneum and are a major lipid constituent of the lamellar sheets present in the intercellular spaces of stratum corneum. These lamellar sheets are thought to provide the epidermal barrier property (27–29). The ceramides in skin are shown to be structurally heterogeneous and can be fractionated into two general classes (30, 31): those that contain amide-linked α-hydroxy fatty acids (HFA) and those that contain amide-linked non-hydroxylated fatty acids (NFA). Also, there is a variability of acyl chain length and degree of sphingosine hydroxylation which provides a large variety of ceramide species. It has been suggested that the hydroxylated fatty acid and sphingosine base associate intermolecularly to increase lateral interactions via hydrogen bonds and thus, impart greater stability to the membrane. It is interesting to note that in tissues where there is pronounced mechanical stress (e.g., kidney, intestine) higher contents of hydroxylated ceramide are found (32).

Although the biological importance of the ceramides, in epidermis and cellular processes, is well established, relatively little effort has been made towards elucidating the physico-chemical properties of ceramides. A study of the thermotropic behavior of anhydrous tetracosanoyl-phytosphingosine indicates that the ceramide can form six crystalline phases depending upon the conditions of crystallization (33). Only one case was observed in which the two hydrocarbon chains parallel stacked in a double layer arrangement in which the longer C24:0 fatty acid chain interdigitates with the sphingosine chain of the other molecule in the opposing leaflet (33, 34). However, there is essentially no information concerning the physical properties of hydrated ceramides. A recent study of natural HFA ceramide (derived from bovine brain cerebrosides) and its interaction with cholesterol suggested that hydrated HFA ceramide forms lamellar arrays (35). Here we compare the structural and thermotropic properties of natural HFA-CER and NFA-CER, derived from bovine brain cerebrosides, using X-ray diffraction and differential scanning calorimetry (DSC) techniques.

MATERIALS AND METHODS

Natural α-hydroxy and non-hydroxy fatty acid ceramides (HFA-CER and NFA-CER respectively; derived from the bovine brain cerebrosides) were obtained in the lyophilized form from Matreya Inc. (Pleasant Gap, PA). Silica gel 60 (0.040–0.063) was obtained from E. Merck (Darmstadt, Germany). Teflon membranes with 0.5-micron pores were obtained from Alltech (Deerfield, IL).

NFA-CER was purified by column chromatography on silica gel 60 eluting isocratically with MeOH–CH_2Cl_2 3.5:96.5 (v/v). Purities of the fractions were checked by thin-layer chromatography (TLC) on Silica gel 60 eluting with MeOH–CH_2Cl_2 5:95 (v/v). Pure fractions (R_f = 0.22) were combined and the solvent was removed by vacuum rotary evaporation. The white solid was dissolved in CH_2Cl_2, filtered through a 0.5-μm Teflon membrane and lyophilized from *t*-butanol. HFA-CER was purified by column chromatography on silica gel 60 eluting isocratically with MeOH–CH_2Cl_2 6:94 (v/v). Purities of the fractions were checked by TLC on Silica gel 60 eluting with MeOH–CH_2Cl_2 7.5:92.5 (v/v). Pure fractions (R_f = 0.26) were combined and solvent was removed by vacuum rotary evaporation. The white solid was redissolved in MeOH–CH_2Cl_2 6:94, filtered through a 0.5-μm teflon membrane, and lyophilized from *t*-butanol. Fatty acid analysis of the NFA-CER ceramide using gas chromatography (36) showed that the principal chain lengths for the amide-linked fatty acids are C:24, C:22, and C:18.

Details of both the preparation of hydrated samples of NFA-CER and HFA-CER and the differential scanning calorimetry (DSC) and X-ray diffraction techniques used for their study are as described in the accompanying paper (37).

RESULTS

Thermotropic behavior of HFA-CER

DSC heating curves of HFA-CER at different hydrations are shown in **Fig. 1.** On heating from 0°C, anhydrous ceramide (Fig. 1, curve a) showed a single, endothermic transition at 94.6°C (ΔH = 15.3 kcal/mol). At 3.8% hydration (Fig. 1, curve b), two overlapping endothermic transitions were observed at 82.3°C and 86.4°C. This was followed by a minor endothermic transition at 95.6°C. On increasing the hydration to 8.0% water (Fig. 1, curve c), the transition temperatures of the overlapping transitions decreased to 82.4°C and 86.0°C; the high temperature transition at 95.6°C was still present. On further increasing the hydration to 12.0% water (Fig. 1, curve d), the high temperature peak disappeared and

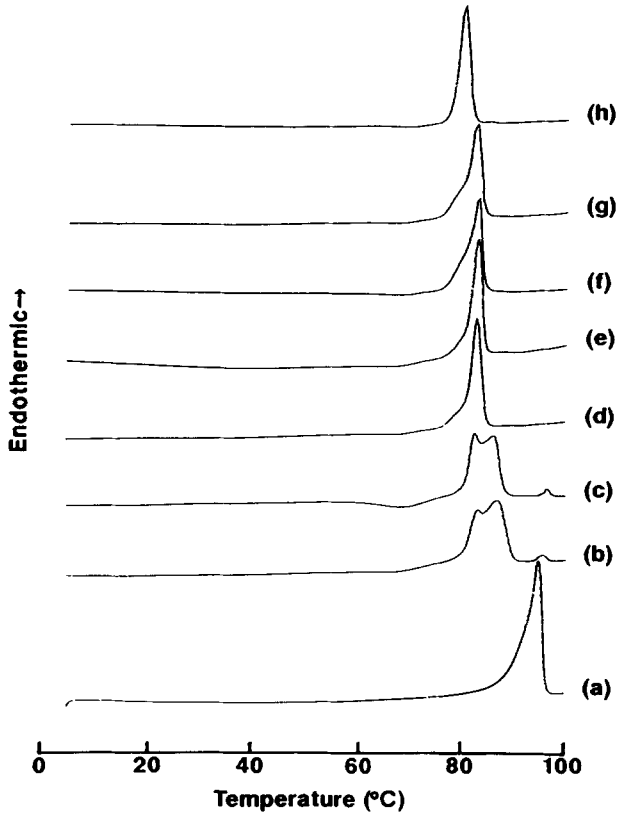

Fig. 1. DSC heating scans of HFA-CER at different hydrations (wt% water): (a) 0% water; (b) 3.8% water; (c) 8.0% water; (d) 12.0% water; (e) 23.1% water; (f) 34.0% water; (g) 49.0% water; and (h) 73.5% water. The heating rate was 5°C/min.

only one endothermic transition was observed at 82.7°C (ΔH = 8.6 kcal/mol). On increasing the hydration from 12.0% to 73.5% water (Fig. 1, curves d–h), the transition temperature decreases to a limiting value (80.0°C). At 73.5% water (Fig. 1, curve h), a single endothermic transition was observed at 80.0°C (ΔH = 8.5 kcal/mol).

For HFA-CER, the effect of hydration on the transition temperature (Tm) and the enthalpy (ΔH) is depicted in **Fig. 2.** On increasing hydration from 0% water to 12.0% water, the transition temperature decreased from 94.6°C to 82.0°C (Fig. 2A; only the high temperature transition was taken in account). No significant change in the transition temperature was observed with further hydration. The transition enthalpy (combined enthalpy where two overlapping transitions are present) exhibited a similar hydration dependence (Fig. 2B). On increasing hydration from 0% water to 12.0% water, the transition enthalpy decreased from 15.3 kcal/mol to 8.5 kcal/mol. These data indicate that HFA-CER can incorporate at least up to 12 wt% of water, as evidenced by the hydration dependence of the thermodynamic parameters Tm and ΔH.

On cooling, anhydrous HFA-CER showed a single exothermic transition at 86.8°C (ΔH = 13.7 kcal/mol). With increasing hydration the exothermic transitions shifted to lower temperature (data not shown) and for fully hydrated HFA-CER (73.5 wt% water) the transition temperature occurred at 75.4°C (ΔH = 8.3 kcal/mol; **Fig. 3,** curve b).

The reversibility of the thermal transition of fully hydrated HFA-CER is illustrated in Fig. 3. On heating, a single endothermic transition was observed at 80.0°C (ΔH = 8.5 kcal/mol, Fig. 3, curve a). Subsequent cooling showed a single exothermic transition at 75.4°C (ΔH = 8.3 kcal/mol; Fig. 3, curve b). On immediate reheating HFA-CER exhibited a heating scan (Fig. 3, curve c) identical to the initial heating scan (Fig. 3, curve a). These data indicate that the transition of fully hydrated HFA-CER is reversible.

X-ray diffraction of HFA-CER

X-ray diffraction was used to determine the structures of the various phases of anhydrous and hydrated HFA-CER. X-ray diffraction of anhydrous HFA-CER at 26°C (**Fig. 4A**), below the transition temperature, showed lamellar reflections in the low-angle region, correspond-

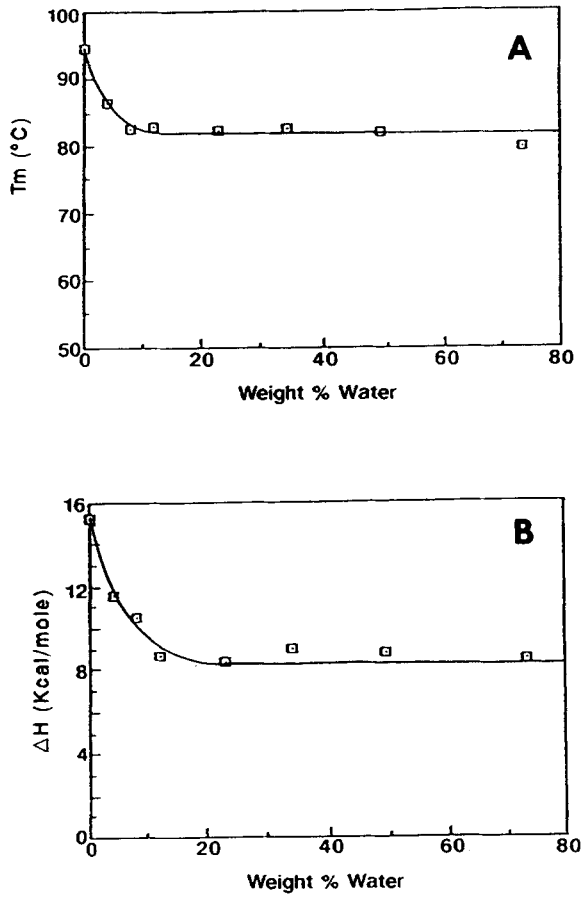

Fig. 2. The effect of hydration on the transition temperature (A) and enthalpy (B) of HFA-CER.

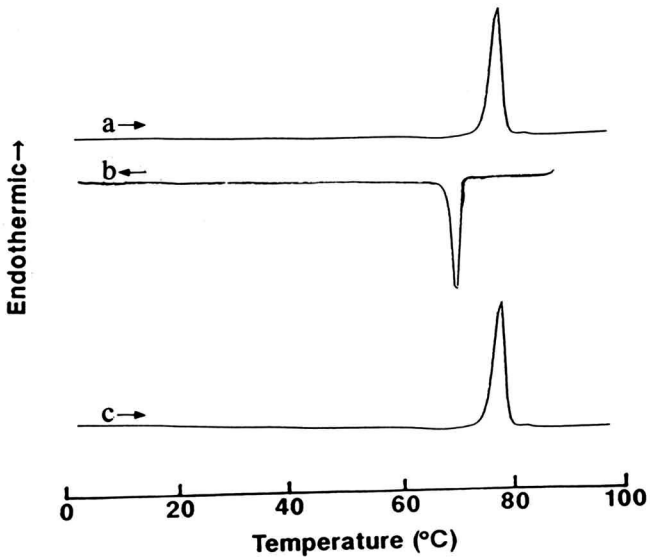

Fig. 3. DSC heating scans of fully hydrated HFA-CER (73.5 wt% water) (a) Heating curve; (b) corresponding cooling curve; and (c) immediate reheating curve. Heating/cooling rates, 5°C/min.

ing to a lamellar repeat distance, d, of 54.1 Å. The wide-angle region showed three strong reflections at 4.3 Å, 4.0 Å, and 3.7 Å (arrow) characteristic of well-ordered chain packing. When anhydrous HFA-CER was heated past the transition to 97°C, the diffraction pattern changed (Fig. 4B). The low-angle region showed a single strong reflection at 33.3 Å (arrow), indicating a disordered phase. However, the presence of a single reflection does not allow the lattice type (lamellar, hexagonal, etc.) to be unequivocally defined. The wide angle-region showed a diffuse band centered at 4.5 Å (arrowed), indicative of a melted chain phase. The X-ray diffraction pattern recorded after immediately cooling to 26°C (data not shown) was essentially identical to that shown in Fig. 4A, indicating the reversibility of the chain melting transition.

X-ray diffraction patterns of fully hydrated HFA-CER (74 wt% water) were also recorded at temperatures below and above the endothermic transition. At 26°C (**Fig. 5A**), the low-angle region showed several reflections characteristic of lamellar phase, d = 60.7 Å. The wide-angle region exhibited a single strong reflection at 4.2 Å, indicative of a gel phase with hexagonal chain packing. X-ray diffraction at 91°C (above the thermal transition) showed low-angle reflections at 44.1 Å, 27.2 Å, 23.1 Å, and 17.4 Å (arrowed) indexing in hexagonal (H_I or H_{II}) geometry (Fig. 5B). The wide-angle region was characterized by a broad diffuse band centered at 4.6 Å (arrowhead), characteristic of melted hydrocarbon chains. Cooling to 26°C resulted in an X-ray diffraction pattern (not shown) identical to that shown in Fig. 5A, indicating the reversibility of the bilayer gel→hexagonal phase transition.

Thermotropic behavior of NFA-CER

Representative DSC heating scans of NFA-CER at different hydrations are shown in **Fig. 6.** The heating scan of anhydrous NFA-CER, over the range 0–100°C, exhibited two endothermic transitions (Fig. 6, curve a) at 81.3°C (ΔH = 6.8 kcal/mol) and at 85.9°C (ΔH = 3.5 kcal/mol). With increasing hydration both transitions shifted progressively to lower temperatures. At 30% hydration (Fig. 6, curve b), the two endothermic transitions appeared at 73.8°C (ΔH = 5.1 kcal/mol) and 84.2°C (ΔH = 5.8 kcal/mol). On further increasing the

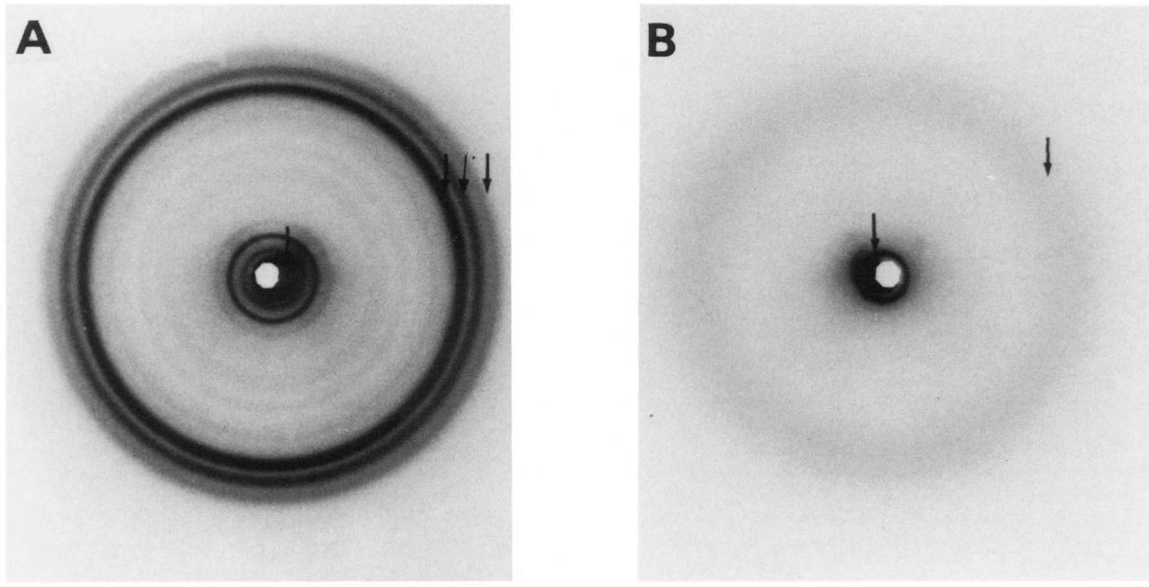

Fig. 4. X-ray diffraction patterns of anhydrous HFA-CER at: (A) 26°C and (B) 97°C.

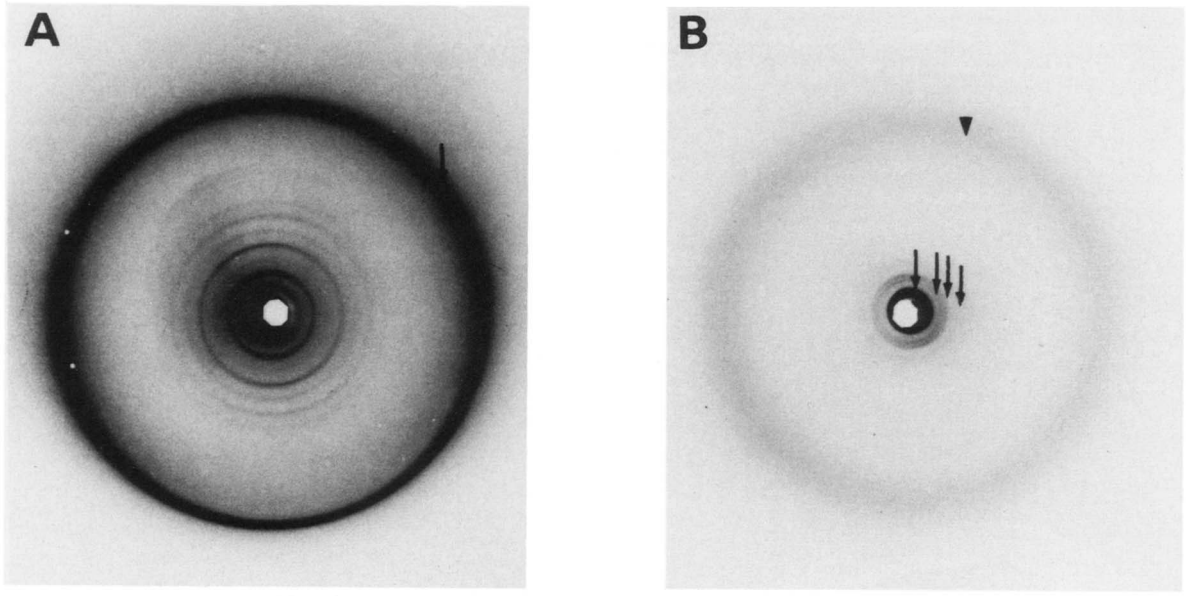

Fig. 5. X-ray diffraction patterns of 74.0% hydrated HFA-CER at: (A) 26°C and (B) 91°C.

hydration to 52% water (Fig. 6, curve c) two well-resolved endothermic transitions appeared at 72.7°C (ΔH = 9.8 kcal/mol) and 81.1°C (ΔH = 4.0 kcal/mol). On further increasing the hydration (74.4% water), no change in the calorimetric behavior was observed (Fig. 6, curve d).

On cooling (data not shown), DSC of anhydrous NFA-CER showed two overlapping exothermic transitions at 69.5°C and 72.9°C (combined ΔH = 10.8 kcal/mol). On increasing the hydration from 0–52 wt% water, both transitions shifted progressively to lower temperatures reaching limiting temperatures of 61.2°C and 64.9°C (combined ΔH = 12.6 kcal/mol), respectively (data not shown). On further increasing the hydration to 74.4% water, no change in the cooling curve was observed (**Fig. 7,** curve b).

The polymorphic phase behavior of fully hydrated NFA-CER is depicted in Fig. 7. The initial DSC heating scan (Fig. 7, curve a) showed two endothermic transitions at 72.7°C (ΔH = 9.8 kcal/mol) and 81.1°C (ΔH = 4.0 kcal/mol). On cooling (Fig. 7, curve b) an exothermic transition was observed at 64.9°C with a shoulder at 61.2°C (combined ΔH = 12.6 kcal/mol). On heating

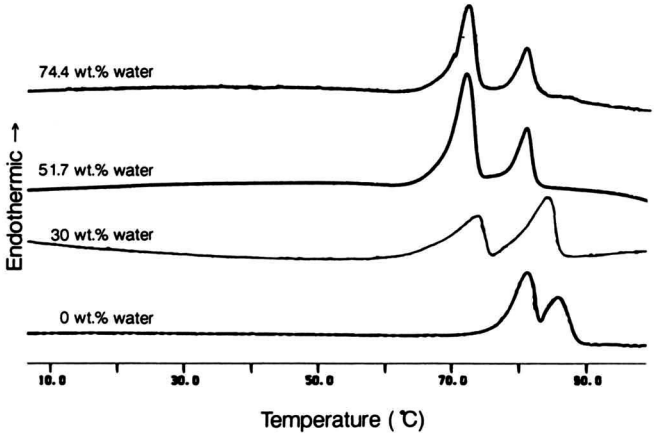

Fig. 6. DSC heating scans of NFA-CER at different hydrations (wt% water): (a) 0% water; (b) 30% water; (c) 51.7% water; and (d) 74.4% water. The heating rate was 5°C/min for all the scans.

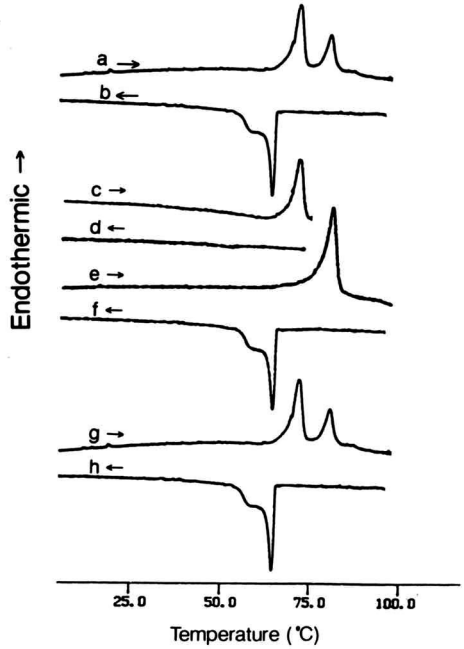

Fig. 7. Polymorphic phase behavior of fully hydrated (74.4 wt% water) NFA-CER: (a) DSC heating scan from 0°C to 100°C; (b) DSC cooling scan from 100°C to 0°C; (c) heating from 0°C to 77°C; (d) cooling back to 0°C; (e) immediate reheating from 0°C to 100°C; (f) cooling from 100°C to 0°C; (g) following heating scan; and (h) immediate cooling scan.

the sample to 77°C (past the first endothermic transition; Fig. 7, curve c) and cooling (Fig. 7, curve d), no exothermic transition was observed indicating that no phase change occurs during cooling. Subsequent heating of the sample to 100°C (Fig. 7, curve e) showed only one endothermic transition at 81.8°C (ΔH = 10.4 kcal/mol). Interestingly, the enthalpy of this transition (ΔH = 10.4 kcal/mol) was much higher than the enthalpy of the corresponding transition (ΔH = 4.0 kcal/mol) observed in the initial scan (Fig. 7, curve a). On subsequent cooling from 100°C to 0°C, the original exothermic transition was observed (Fig. 7, curves f and b). The subsequent heating (Fig. 7, curve g) and cooling (Fig. 7, curve h) scans were identical to the initial heating (Fig. 7, curve a) and cooling (Fig. 7, curve b) scans, indicating that the initial phase behavior was reproducible after cooling from temperatures >82°C.

X-ray diffraction of NFA-CER

X-ray diffraction patterns of anhydrous and hydrated NFA-CER were recorded at temperatures below and above the observed calorimetric transitions to determine the structures of the various phases. For anhydrous NFA-CER at 26°C, the low-angle region showed

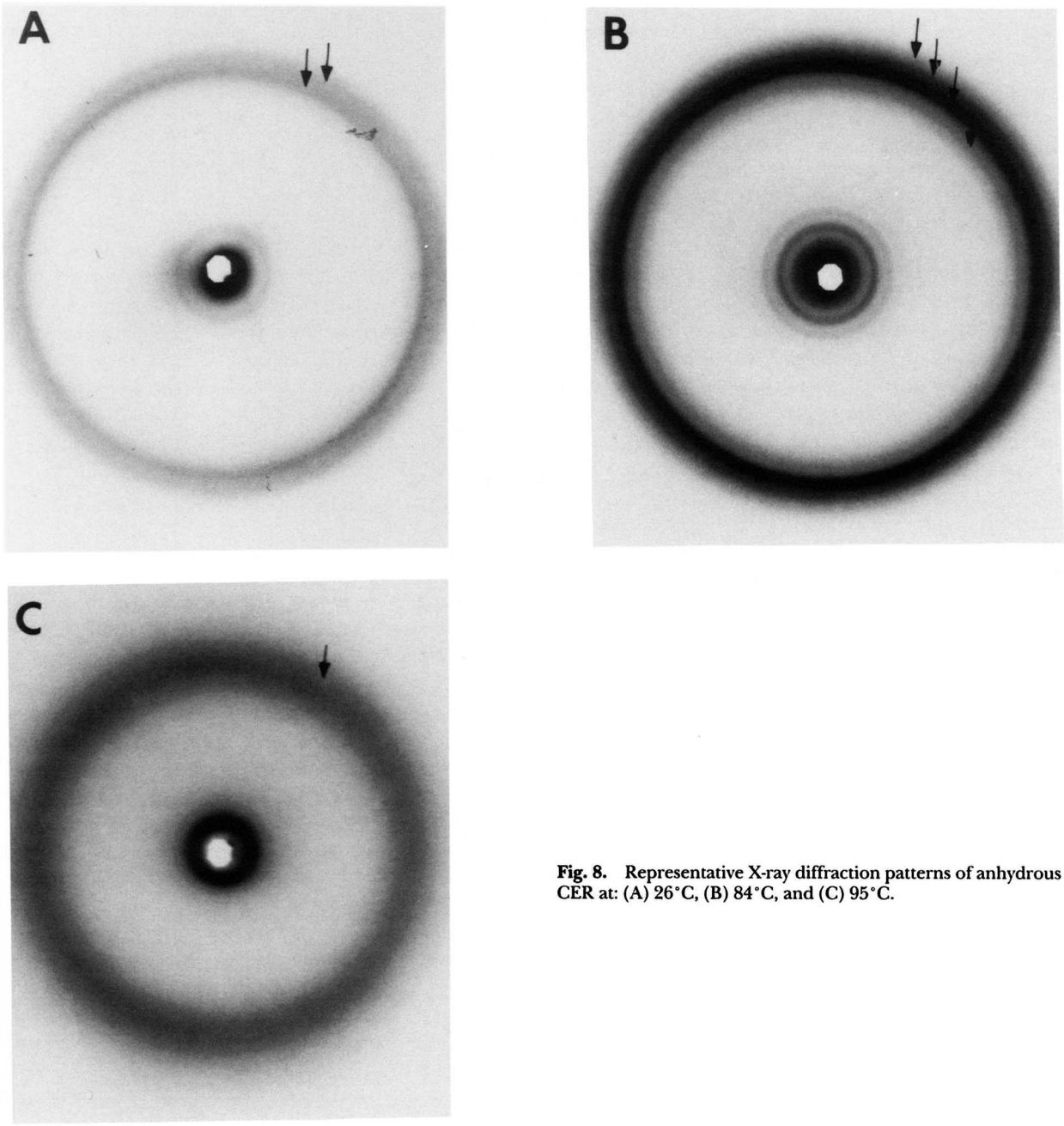

Fig. 8. Representative X-ray diffraction patterns of anhydrous NFA-CER at: (A) 26°C, (B) 84°C, and (C) 95°C.

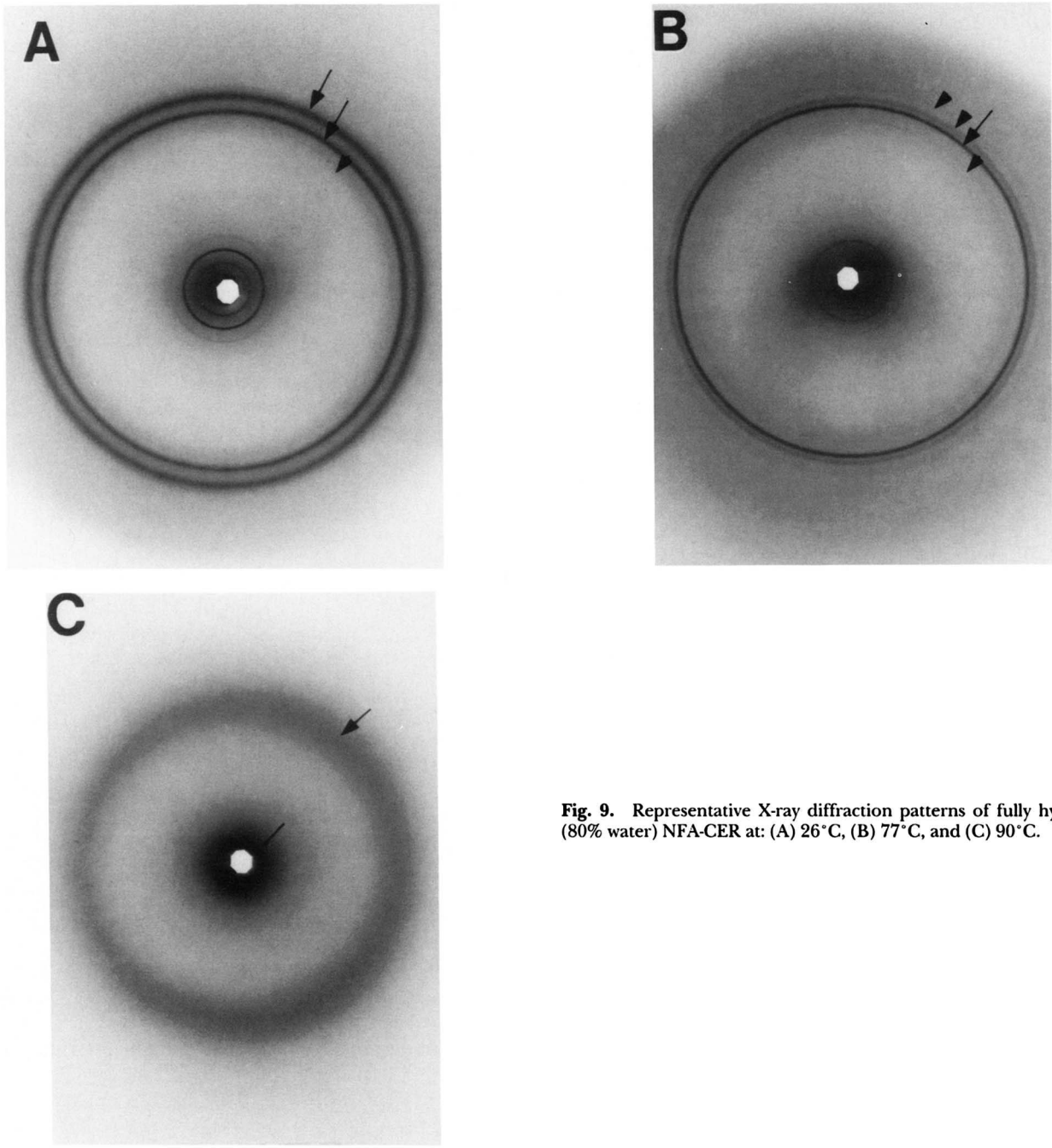

Fig. 9. Representative X-ray diffraction patterns of fully hydrated (80% water) NFA-CER at: (A) 26°C, (B) 77°C, and (C) 90°C.

lamellar reflections corresponding to a bilayer repeat distance of 56.0 Å (**Fig. 8A**). The wide-angle region showed two reflections (arrowed) at 4.2 Å and 4.0 Å. On heating to 84°C (past the first endothermic transition), the diffraction pattern changed slightly (Fig. 8B). The low-angle region still showed the presence of a lamellar structure but with a reduced bilayer periodicity of 52.0 Å. In the wide-angle region four reflections (arrowed) were observed at 4.4 Å, 4.1 Å, 3.9 Å, and 3.7 Å, indicating an ordered phase. On cooling from 84°C to 26°C, the diffraction pattern (not shown) remained essentially same as that shown in Fig. 8B. Above the second thermal transition (at 95°C), the low-angle region in the diffraction pattern exhibited a single strong reflection at 31.3 Å, indicative of a disordered phase. The wide-angle region showed a broad reflection at 4.5 Å (arrow head) characteristic of melted-chain phase. On cooling from 95°C to 26°C, the diffraction pattern

(not shown) was similar to that of Fig. 8A.

The X-ray diffraction pattern of fully hydrated (80% water) NFA-CER, at 26°C, showed reflections in the low-angle region corresponding to a lamellar bilayer periodicity of 58.6 Å (**Fig. 9A**). The wide-angle region showed two strong reflections at 3.8 Å and 4.2 Å (arrowed), and a weak reflection at 4.6 Å (indicated by arrow heads). On heating the sample past the first endothermic transition (77°C), the X-ray diffraction pattern showed low-angle reflections, still corresponding to a lamellar structure although with a reduced bilayer periodicity of 53.1 Å (Fig. 9B). The wide-angle region showed a strong sharp reflection at 4.0 Å (arrowed) and three weaker reflections at 4.6 Å, 4.2 Å, and 3.8 Å (indicated by arrow head), again indicating a well-ordered phase. On cooling back to 26°C, the diffraction pattern (not shown) was identical to the recorded at 77°C (Fig. 9B), indicating that on cooling the first endothermic transition is irreversible. The X-ray diffraction pattern at 90°C (above the second endothermic transition) showed a single reflection in the low-angle region at 30.0 Å (Fig. 9C) and a diffuse band at 4.6 Å, (arrow head) again indicative of a melted-chain phase.

DISCUSSION

The calorimetric studies of HFA-CER demonstrated that its thermotropic behavior changes with hydration. HFA-CER showed a simple, reversible thermal behavior for both the anhydrous and hydrated forms. Anhydrous HFA-CER exhibits a reversible transition at 95.4°C (ΔH = 15.3 kcal/mol; Fig. 1). On increasing the hydration to 12% water, the transition temperature progressively lowered from 95.4°C to 80.0°C and the transition enthalpy decreased from 15.3 kcal/mol to 8.5 kcal/mol (Fig. 2A and B). This suggests that HFA-CER can hydrate approximately up to 12% water.

The X-ray diffraction pattern of anhydrous HFA-CER taken at 26°C (Fig. 4A) showed numerous lamellar reflections in the low angle region, corresponding to a bilayer periodicity of 54.1 Å. Bovine brain ceramide has an abundance of C22 and C24 hydrocarbon chains and the expected chain length for one molecule would be approximately 26.25 Å and 28.75 Å, respectively. The observed bilayer distance is slightly smaller than the sum of two chain lengths and head groups (approximately 4 Å each; see ref. 33). Probably, HFA-CER is able to form a partially interdigitated bilayer where the amide-linked fatty acid chain (chain length = 28.75 Å) of one molecule lies against the sphingosine chain (chain length = 21.25 Å) of the other ceramide molecule. This may account for a bilayer periodicity of ~58 Å. The small discrepancy in the observed and calculated periodicities can be explained by chain tilting relative to the bilayer normal. The wide-angle region displayed reflections at 4.3 Å, 4.0 Å, and 3.7 Å suggestive of a crystalline chain packing mode.

Increasing the temperature to 97°C (above the main transition), the X-ray diffraction pattern displayed a diffuse wide reflection at 4.5 Å, indicative of melted hydrocarbon chains (Fig. 4B). The low-angle region showed a single strong reflection at 33.3 Å, indicating of long-range (stacking/packing) disorder, in addition to the short-range (chain-packing) disorder. However, the presence of a single low-angle reflection does not allow the geometry of the matrix (lamellar, hexagonal, melt, etc.) to be determined. Cooling to 26°C produced a diffraction pattern (not shown) identical to the initial one (Fig. 4A), indicating that the thermal transition of anhydrous HFA-CER is reversible, consistent with the DSC data (see Fig. 3).

X-ray diffraction of fully hydrated (74% water) HFA-CER at 26°C (Fig. 5A) showed a lamellar phase with a bilayer periodicity of 60.7 Å, ~6 Å greater than anhydrous HFA-CER (d = 54.1 Å). This difference in the bilayer periodicities of the anhydrous and hydrated forms is presumably due to the additional water layer between the lamellar sheets and/or a reduction in chain tilt relative to the bilayer normal. The wide-angle region showed a single wide reflection at 4.2 Å indicative of a hexagonal chain packing. This is a less specific type of chain packing and is probably due to the disruption/weakening of lateral interactions between ceramide molecules due to water–ceramide interactions at the bilayer interface. Thus, at low temperature, anhydrous HFA-CER forms bilayers with crystalline chain packing, whereas the hydrated bilayers show the less specific, hexagonal chain packing.

Above the chain-melting transition at 91°C (Fig. 5B), low-angle reflections corresponding to a hexagonal phase are observed. This non-bilayer phase has also been observed in other lipids with small or non-polar headgroups and is possibly involved in membrane fusion and modulation of protein activity (38–41). However, at this point, we cannot conclude whether the gel phase converts directly to hexagonal phase ($L_\beta \rightarrow H_{II}$) or it converts to an L_α phase stable over a small temperature range which then converts to the hexagonal phase ($L_\beta \rightarrow L_\alpha \rightarrow H_{II}$). In any case, both the X-ray diffraction and DSC data confirm that the ($L_\beta \rightarrow H_{II}$) transition is reversible, the original bilayer phase being re-formed on cooling. Thus, the DSC and X-ray diffraction data indicate that anhydrous and HFA-CER show simple, reversible phase behavior. Low temperature incubation for short time periods does not affect the subsequent calorimetric behavior, suggesting the gel phase is quite stable. Although longer incubations could possibly con-

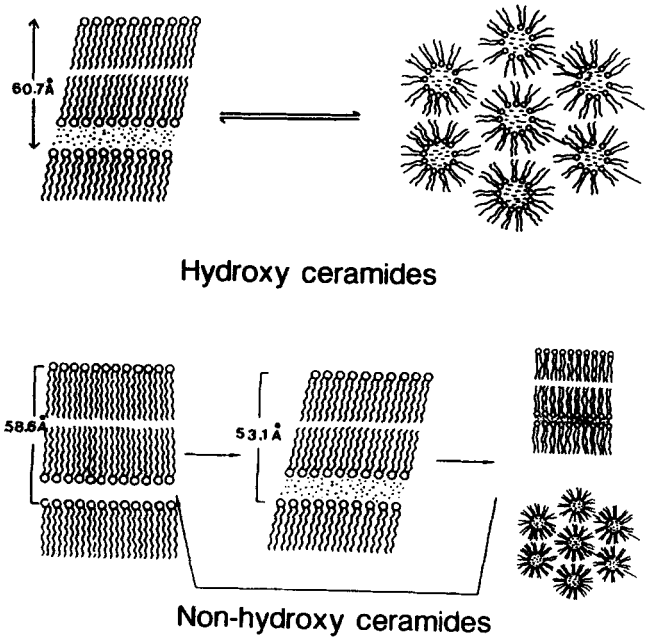

Fig. 10. Summary of the phase behavior of fully hydrated HFA-CER and NFA-CER.

vert hydrated HFA-CER to a more stable gel phase characterized by a more ordered chain packing mode as observed for synthetic cerebroside sulfate (42), the chain heterogeneity of HFA-CER is probably going to inhibit this process.

The calorimetric studies of NFA-CER indicate that this mixed-chain ceramide showed a more complex phase behavior with two transitions observed at all hydrations (0–74% water; Fig. 6), the transition temperatures decreasing on increasing hydration. When fully hydrated (74.4% H_2O) NFA-CER was heated past the first endothermic transition (77°C) and cooled, no exothermic transition was observed (Fig. 7, curve d). This indicates that the phase transition undergone during the first endothermic transition is irreversible on cooling. On reheating the sample to 100°C, a single endothermic transition is observed at 81.1°C (ΔH = 10.4 kcal/mol) with increased enthalpy (Fig. 7, curve e), indicating the presence of a well-ordered phase exhibiting a high transition enthalpy on chain-melting. The calorimetric behavior suggests that the initial, lower melting bilayer gel phase is in fact metastable with respect to the second, higher melting gel phase, although no exothermic event is observed between the two calorimetric transitions. However, the wide-angle X-ray diffraction data do suggest that the high-melting bilayer phase has a more ordered chain packing mode than the low-melting phase (see Fig. 9A, B).

A similar protocol was followed to record the X-ray diffraction patterns. On heating, the anhydrous NFA-CER showed two endothermic transitions, indicating the presence of three phases. The phase present at 26°C is a bilayer gel phase with a periodicity of 56.0 Å (Fig. 8A). At 84°C, a more ordered bilayer phase with a reduced periodicity of 52.0 Å with crystalline chain packing is present (Fig. 8B). On cooling anhydrous NFA-CER from 84°C to 26°C, the diffraction pattern (not shown) was identical to that shown in Fig. 8B, indicating that no phase change occurs during cooling. Above the second transition, a disordered melted-chain phase of undefined geometry is present (Fig. 8C).

DSC heating scans of fully hydrated NFA-CER (74.4% water) also suggested the presence of three phases (Fig. 6, curve d). X-ray diffraction at 26°C (below the first endothermic transition) showed a bilayer structure, periodicity = 58.6 Å with an ordered, crystalline chain packing (Fig. 9A). Above the first transition at 77°C, a bilayer structure with a reduced bilayer periodicity of 53.1 Å and a well-ordered crystalline chain packing is present (Fig. 9B). Possible explanations for the reduced bilayer periodicity would be an increased tilt of the ceramide molecule relative to the bilayer normal and/or a reduction in the hydration layer. On cooling from 77°C to 26°C, the diffraction pattern is essentially identical to that of Fig. 9B. This indicates that the first endothermic transition (Tm = 72.7°C) of NFA-CER is irreversible on cooling, consistent with the DSC data. Above the second transition (95°C) the single low-angle reflection at 30.0 Å and a diffuse reflection at 4.6 Å (Fig. 9C) is indicative of a disordered, melted-chain phase. Thus, NFA-CER exhibits polymorphic behavior with two low temperature bilayer gel phases. One phase (bilayer periodicity = 58.6 Å) is produced upon cooling the sample from the melted-chain phase and is stable from 0 to 73°C. The second bilayer phase (periodicity = 53.1 Å) is produced upon heating NFA-CER to 77°C and then cooling. This bilayer phase is stable over the temperature range 0 to 80°C and undergoes chain-melting to the high temperature, disordered phase.

In summary, HFA-CER exhibits a simple phase behavior that involves the interconversion of bilayer gel and hexagonal melted-chain phases (**Fig. 10**). However, NFA-CER shows a more complex polymorphic phase behavior. On heating, NFA-CER converts from a gel phase (perhaps metastable) to a more stable gel phase before going through the chain melting transition. Presumably the presence of the α-hydroxy group in HFA-CER prevents the formation of multiple phases. A similar type of phase behavior is shown by natural bovine brain cerebrosides; the hydroxy cerebroside fraction shows a simple phase behavior whereas the non-hydroxy cerebroside fraction displays a complex polymorphic phase behavior (7). It seems reasonable to suggest that increased hydrogen bonding involving the α-hydroxy group is responsible for the simpler phase behavior of

HFA-ceramides and cerebrosides. Studies of synthetic cerebroside sulfate have suggested that hydroxylation leads to increased intermolecular interactions which in some way inhibits formation of a stable state (42).

We are grateful to Dr. Richard I. Duclos, Jr. for his help in purifying the ceramides. We also thank Mr. J. Owusu-Djamboe for technical help and Dr. D. Atkinson for valuable advice. This research is supported by research grant HL 26335 from the National Institutes of Health and a grant from Unilever Research.

Manuscript received 6 February 1995 and in revised form 23 May 1995.

REFERENCES

1. Roseman, S. 1970. The synthesis of complex carbohydrates by multiglycosyltransferase systems and their potential function in intercellular adhesion. *Chem. Phys. Lipids.* **5:** 270–297.
2. Rapport, M. M., and L. Graf. 1969. Immunochemical reactions of lipids. *Prog. Allergy.* **13:** 273–331.
3. Harouse, J. M., S. Bhat, S. L. Spitalnik, M. Laughlin, K. Stefano, D. H. Silberberg, and F. Gonalzo-Scarano. 1992. Inhibition of entry of HIV-1 in neutral cell lines by antibodies against galactosylceramide. *Science.* **253:** 320–322.
4. Nilsson, G. 1992. Carbohydrate antigens in human lung carcinoma. *APMIS Suppl.* **27:** 149–161.
5. Saito, T., and H. Ochiai. 1993. Evidence for a glycolipid anchor of gp64, a putative cell–cell adhesion protein of Polysphondylium pallidum. *Eur. J. Biochem.* **218:** 623–628.
6. Wiegandt, H. 1992. Insect glycolipids. *Biophys. Biochim. Acta.* **1123:** 117–126.
7. Curatolo, W. 1982. Thermal behavior of fractionated and unfractionated bovine brain cerebrosides. *Biochemistry.* **21:** 1761–1772.
8. Hoekstra, D., and J. W. Kok. 1992. Trafficking of glycosphingolipids in eukaryotic cells: sorting and recycling of lipids. *Biophys. Biochim. Acta.* **1113:** 277–294.
9. Jeckel, D., A. Karrenbauer, R. Birk, R. R. Schmidt, and F. Wieland. 1990. Glucosylceramide is synthesized at the cytosolic surface of various Golgi subfractions. *FEBS Lett.* **261:** 155–157.
10. Schutze, S., K. Potthoff, T. Machleidt, D. Berkovic, K. Wiegmann, and M. Kronke. 1992. TNF activates NF-κB by phosphatidylcholine-specific phospholipase C-induced "acidic" sphingomyelin breakdown. *Cell.* **71:** 765–776.
11. Kim, M. Y., C. Linardic, L. Obeid, and Y. A. Hannun. 1991. Identification of sphingomyelin turnover as an effector mechanism for the action of tumor necrosis factor alpha and gamma-interferon. *J. Biol. Chem.* **266:** 484–489.
12. Okazaki, T., R. M. Bell, and Y. A. Hannun. 1989. Sphingomyelin turnover induced by vitamin D_3 in HL-60 cells. Role in cell differentiation. *J. Biol. Chem.* **264:** 19076–19080.
13. Okazaki, T., A. Bielawaski, R. M. Bell, and Y. A. Hannun. 1990. Role of ceramide as a lipid mediator of 1α, 25-dihydroxyvitamin D_3-induced HL-60 cell differentiation. *J. Biol. Chem.* **265:** 15823–15831.
14. Dobrowski, R. T., and Y. A. Hannun. 1992. Ceramide activates a cytosolic phosphatase. *J. Biol. Chem.* **267:** 5048–5051.
15. Goldkorn, T., K. A. Dressler, J. Muindi, N. S. Radin, J. Mendelsohn, D. Menaldins, D. Liotta, and R. N. Kolesnick. 1991. Ceramide stimulates epidermal growth factor receptor phosphorylation in A431 human epidermoid carcinoma cells. Evidence that ceramide may mediate sphingosine action. *J. Biol. Chem.* **266:** 16092–16097.
16. Obeid, L. M., C. M. Linardic, L. A. Karolak, and Y. A. Hannun. 1993. Programmed cell death induced by ceramide. *Science.* **259:** 1769–1771.
17. Kalen, A., R. A. Borchardt, and R. M. Bell. 1992. Elevated ceramide levels in GH4C1 cells treated with retinoic acid. *Biochim. Biophys. Acta.* **1125:** 90–96.
18. Pagano, R. E. 1990. The Golgi apparatus: insights from lipid biochemistry. *Biochem. Soc. Trans.* **18:** 361–366.
19. Rosenwald, A. G., and R. E. Pagano. 1993. Inhibition of glycoprotein traffic through the secretory pathway by ceramide. *J. Biol. Chem.* **268:** 4577–4579.
20. Joseph, C. K., H. S. Byun, R. Bittman, and R. N. Kolesnick. 1993. Substrate recognition by ceramide-activated protein kinase. *J. Biol. Chem.* **268:** 20002–20006.
21. Raines, M. A., R. N. Kolesnick, and D. W. Golde. 1993. Sphingomyelinase and ceramide activate mitogen-activated protein kinase. *J. Biol. Chem.* **268:** 14572–14575.
22. Dobrowsky, R. T., and Y. A. Hannun. 1993. Ceramide-activated protein phosphatase: partial purification and relationship to protein phosphatase 2A. *Adv. Lipid Res.* **25:** 91–104.
23. Dobrowsky, R. T., C. Kamibayashi, M. C. Mumby, and Y. A. Hannun. 1993. Ceramide activates heterotrimeric protein phosphatase 2A. *J. Biol. Chem.* **268:** 15523–15530.
24. Fishbein, J. D., R. T. Dobrowsky, A. Bielawska, S. Garrett, and Y. A. Hannun. 1993. Ceramide-mediated growth inhibition and CAPP are conserved in *Saccharomyces cerevisiae*. *J. Biol. Chem.* **268:** 9255–9261.
25. Elias, P. M., and D. S. Friend. 1975. The permeability barrier in mammalian epidermis. *J. Cell Biol.* **65:** 180–191.
26. Elias, P. M., J. Goerke, and D. S. Friend. 1977. Mammalian epidermal barrier lipid layers: composition and influence on structure. *J. Invest. Dermatol.* **69:** 535–546.
27. Gray, G. M., and H. J. Yardley. 1975. Different populations of pig epidermal cells: isolation and lipid composition. *J. Lipid Res.* **16:** 441–447.
28. Gray, G. M., and H. J. Yardley. 1975. Lipid composition of cells isolated from pig, human and rat epidermis. *J. Lipid Res.* **16:** 434–440.
29. Lavker, R. M. 1976. Membrane coating granules: the fate of the discharged lipids. *J. Ultrastruct. Res.* **55:** 79–86.
30. Gray, G. M., and R. J. White. 1978. Glycosphingolipid and ceramides in human and pig epidermis. *J. Invest. Dermatol.* **70:** 336–341.
31. Elias, P. M., B. E. Brown, P. Fritsche, J. Goerke, P. M. Gray, and R. J. White. 1979. Localization and composition of lipids in neonatal mouse stratum granulosum and stratum corneum. *J. Invest. Dermatol.* **73:** 339–348.
32. Karlsson, K. A. 1977. Aspects on structure and function of sphingolipids in cell surface membranes. *Struct. Biol. Membr.* 245–274.
33. Dahlen, B., and I. Pascher. 1972. Molecular arrangements in sphingolipids. Crystal structure of N-tetracosanoylphytosphingosine. *Acta. Crystallogr.* **28:** 2396–2404.
34. Pascher, I., M. Lundmark, P. G. Nyholm, and S. Sundell. 1992. Crystal structure of membrane lipids. *Biochim. Biophys. Acta.* **1113:** 339–373.
35. Wiedmann, T. S., and A. Salmon. 1991. Thermotropic phase behavior of the hydroxyceramide/cholesterol sys-

tem. *Lipids.* **26:** 364–368.
36. Morrison, W. R., and L. M. Smith. 1964. Preparation of fatty acid methyl esters and dimethylacetals from lipids with boron fluoride–methanol. *J. Lipid Res.* **5:** 600–608.
37. Shah, J., J. M. Atienza, R. I. Duclos, A. V. Rawlings, Z. X. Dong, and G. G. Shipley. 1995. Structural and thermotropic properties of synthetic C16:0 (palmitoyl) ceramide: effect of hydration. *J. Lipid Res.* **36:** 1936–1944.
38. Hope, M. J., D. C. Walker, and P. R. Cullis. 1983. Ca^{+} and pH-induced fusion of small unilamellar vesicles consisting of phosphatidylethanolamine and negatively charged phospholipids: a freeze fracture study. *Biochem. Biophys. Res. Commun.* **110:** 15–22.
39. Eastman, S. J., M. J. Hope, K. F. Wong, and P. R. Cullis. 1992. Influence of phospholipid asymmetry on fusion between large unilamellar vesicles. *Biochemistry.* **31:** 4262–4268.
40. Burger, K. N., and A. J. Verkleij. 1990. Membrane fusion. *Experientia.* **46:** 631–644.
41. Epand, R. M. 1987. The relationship between the effects of drugs on bilayer stability and on protein kinase C activity. *Chem. Biol. Interact.* **63:** 239–247.
42. Boggs, J. M., K. M. Koshy, and G. Rangaraj. 1984. Effect of fatty acid chain length, fatty acid hydroxylation, and various cations on phase behavior of synthetic cerebroside sulfate. *Chem. Phys. Lipids.* **36:** 65–89.